ACS APPLIED MATERIALS & INTERFACES

Research Article

www.acsami.org

Encapsulation of Amoxicillin within Laponite-Doped Poly(lactic-*co*-glycolic acid) Nanofibers: Preparation, Characterization, and Antibacterial Activity

Shige Wang,[†,‡] Fuyin Zheng,[§] Yunpeng Huang,[§] Yuting Fang,[‡] Mingwu Shen,[§] Meifang Zhu,[†] and Xiangyang Shi*[,†,§,⊥]

[†]State Key Laboratory for Modification of Chemical Fibers and Polymer Materials, Donghua University, Shanghai 201620, People's Republic of China

[‡]College of Materials Science and Engineering, Donghua University, Shanghai 201620, People's Republic of China

[§]College of Chemistry, Chemical Engineering and Biotechnology, Donghua University, Shanghai 201620, People's Republic of China

[⊥]CQM-Centro de Química da Madeira, Universidade da Madeira, Campus da Penteada, 9000-390 Funchal, Portugal

Supporting Information

ABSTRACT: We report a facile approach to encapsulating amoxicillin (AMX) within laponite (LAP)-doped poly(lactic-*co*-glycolic acid) (PLGA) nanofibers for biomedical applications. In this study, a synthetic clay material, LAP nanodisks, was first used to encapsulate AMX. Then, the AMX-loaded LAP nanodisks with an optimized AMX loading efficiency of 9.76 ± 0.57% were incorporated within PLGA nanofibers through electrospinning to form hybrid PLGA/LAP/AMX nanofibers. The loading of AMX within LAP nanodisks and the loading of LAP/AMX within PLGA nanofibers were characterized via different techniques. In vitro drug release profile, antimicrobial activity, and cytocompatibility of the formed hybrid PLGA/LAP/AMX nanofibers were also investigated. We show that the loading of AMX within LAP nanodisks does not lead to the change of LAP morphology and crystalline structure and the incorporation of LAP/AMX nanodisks does not significantly change the morphology of the PLGA nanofibers. Importantly, the loading of AMX within LAP-doped PLGA nanofibers enables a sustained release of AMX, much slower than that within a single carrier of LAP nanodisks or PLGA nanofibers. Further antimicrobial activity and cytocompatibility assays demonstrate that the antimicrobial activity of AMX toward the growth inhibition of a model bacterium of *Staphylococcus aureus* is not compromised after being loaded into the hybrid nanofibers, and the PLGA/LAP/AMX nanofibers display good cytocompatibility, similar to pure PLGA nanofibers. With the sustained release profile and the reserved drug activity, the organic/inorganic hybrid nanofiber-based drug delivery system may find various applications in tissue engineering and pharmaceutical science.

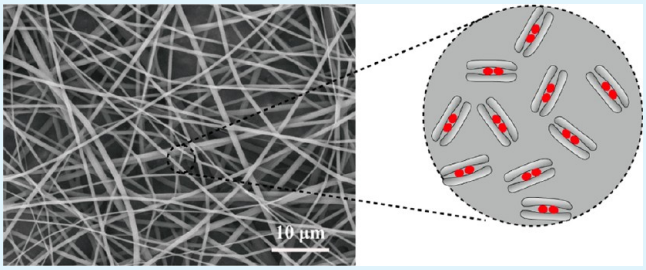

KEYWORDS: *poly(lactic-co-glycolic acid), laponite, electrospinning, amoxicillin, sustained release, antimicrobial activity*

INTRODUCTION

The distinctive features of nanofibers such as flexibility in surface functionalities, superior mechanical durability, and interconnected and readily controlled secondary structures[1−3] afford them to be used as a unique drug delivery system, which has inherent advantages including easy implementation, little influence on the drug activity, and well controlled drug release rate.[4−6] Electrospinning is a simple and straightforward way to produce nanofibers with designed structure and morphology.[3,7−9] Since Kenawy et al. first examined the drug release property from electrospun nanofibers, the use of electrospun nanofibers for drug delivery applications has received increasing interest in the pharmaceutical field.[5,10] Until now, a number of different drug-loading methods have been developed via conventional, emulsion, or coaxial electrospinning techniques.[10−16] In the conventional single fluid electrospinning method, drug molecules are directly integrated within the nanofibers by simply electrospinning the drug/polymer mixture solution or by absorbing/assembling the drugs onto the nanofiber surfaces or in the interior of nanofibers.[11−14] Although this method allows easy incorporation of drug molecules within the nanofibers, a burst release often occurs, which is not desirable in most cases.[10,15] Emulsion and coaxial electrospinning are two improved techniques to be used for drug delivery applications, which is able to mitigate the burst release of the drug to some extent.[13,15,17] In both methods, the drugs are able to be embedded into the core region of the nanofibers in a reservoir-type model and form a so-called

Received: September 27, 2012
Accepted: November 6, 2012
Published: November 6, 2012

Scheme 1. Schematic Illustration of the Loading of Free AMX Drug within PLGA Nanofibers (a) and the Loading of AMX/LAP within PLGA Nanofibers (b)

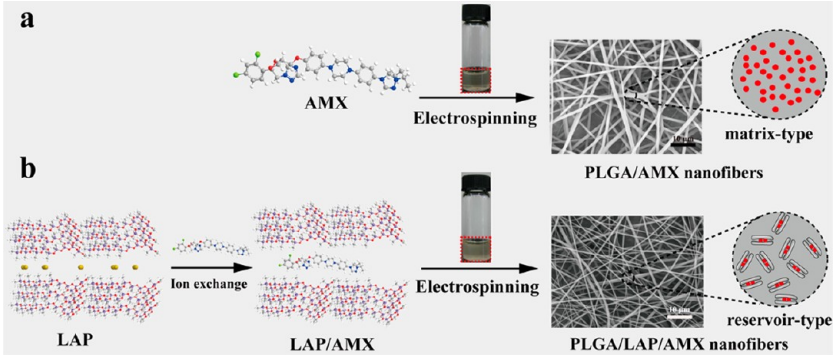

"core–sheath" structure. In this reservoir-type structure, the outer polymer shell can act as an additional barrier to control the drug release profile.[16] Nevertheless, there are still some issues existing in the emulsion and coaxial electrospinning techniques. For example, the coaxial electrospinning may need substantial optimization of the electrospinning parameters, and the emulsifier used in emulsion electrospinning may cause compromised biocompatibility of the nanofibers.[5,16] Therefore, development of other nanofiber systems that can overcome the burst release of the encapsulated drugs still remains a great challenge.

In our previous study, we reported the use of halloysite nanotubes (HNTs)/poly(lactic-*co*-glycolic acid) (PLGA) composite nanofibers for encapsulation and release of a model drug tetracycline hydrochloride (TCH).[5] In this approach, the TCH drug molecules were first physically encapsulated within the HNTs, followed by electrospinning the mixture solution of PLGA and TCH-loaded HNTs to form a composite drug-incorporated nanofiber, which was proven to be able to significantly alleviate the burst release of the TCH. This preliminary success leads us to hypothesize that other naturally occurring or synthetic clay materials that have been used for drug delivery applications may also be able to be incorporated within polymer nanofibers to improve the drug release profile for various biomedical applications. As a synthetic clay material, laponite (LAP) has been used as a drug carrier because the interlayer space of LAP can be used for effective drug encapsulation with high retention capacity.[18−20] For example, Jung et al. reported the incorporation of a hydrophobic drug itraconazole (ITA) into LAP through an interfacial interaction of LAP and ITA. However, their release data showed that the release of ITA from ITA/laponite hybrid could reach 75% during the first 24 h.[18,19] Take the excellent biodegradability, biocompatibility, and electrospinnability of PLGA into account,[21,22] it is expected that PLGA/LAP composite nanofibers may be used as drug carriers to afford the encapsulated drugs with a sustained release profile.

In this present study, LAP nanodisks were first used to encapsulate a model drug of amoxicillin (AMX). Then, the LAP/AMX nanodisks were incorporated within PLGA nanofibers via electrospinning to form PLGA/LAP/AMX nanofibers (Scheme 1). The formed LAP/AMX nanodisks and the composite PLGA/LAP/AMX nanofibers were intensively characterized using different techniques. In vitro drug release behavior of the composite PLGA/LAP/AMX nanofibers was examined using UV–vis spectroscopy. The antimicrobial activity of the composite nanofibers was investigated using *Staphylococcus aureus* (*S. aureus*) as a model bacterium both in liquid and on solid medium. Finally, the cytocompatibility of PLGA/LAP/AMX nanofibers was evaluated through 3-(4,5-dimethylthiazol-2-yl)-2,5-diphenyltetrazolium bromide (MTT) colorimetric assay and scanning electron microscopy (SEM) morphology observation of porcine iliac artery endothelial cells (PIEC) cultured onto the nanofiber scaffold. To our knowledge, this is the first report related to the development of PLGA/LAP composite nanofibers for drug delivery applications.

EXPERIMENTAL SECTION

Materials. PLGA (M_w = 81 000 g/mol) with a lactic acid/glycolic acid ratio of 50:50 and LAP were purchased from Jinan Daigang Biotechnology Co., Ltd. (China) and Zhejiang Institute of Geologic and Mineral Resources (China), respectively. AMX was from Shanghai Yuanye Biotechnology Co., Ltd. *S. aureus* was purchased from Shanghai Fuzhong Biotechnology Development Co., Ltd. Luria-Bertani (LB)-medium and agar were from Beijing Aoboxing Biotechnology Co., Ltd., tetrahydrofuran (THF), and *N*,*N*-dimethylformamide (DMF) were from Sinopharm Chemical Reagent Co., Ltd. (China). PIEC cells were obtained from Institute of Biochemistry and Cell Biology (the Chinese Academy of Sciences, Shanghai). Dulbecco's Modified Eagle's medium (DMEM), fetal bovine serum (FBS), penicillin, and streptomycin were purchased from Hangzhou Jinuo Biomedical Technology (Hangzhou, China). All chemicals and reagents were used as received. Water used in all experiments was purified using a Milli-Q Plus 185 water purification system (Millipore, Bedford, MA) with resistivity higher than 18 MΩ·cm.

Preparation of Drug-Loaded LAP Nanodisks. AMX was first dissolved into water to obtain AMX aqueous solutions with different concentrations (0.1, 0.3, 0.5, 1, and 2 mg/mL, respectively) at room temperature. Then, LAP nanodisks were dispersed into the resulting AMX solutions with different concentrations (3, 5, and 10 mg/mL, respectively) to get a batch of LAP/AMX suspensions. After that, the LAP/AMX suspensions were magnetically stirred for 24 h in order to make the LAP fully swell and to make the AMX molecules be sufficiently intercalated into the interlayer of LAP. The LAP/AMX nanodisks were then separated by centrifugation (8000 rpm, 5 min) and washed with water for 3 times to remove the excessive AMX. The supernatants after 4 times centrifugation were collected together, and the nonencapsulated AMX was quantified using a Lambda 25 UV–vis spectrophotometer (Perkin-Elmer, USA) at 230 nm with a concentration–absorbance calibration curve at the same wavelength. Finally, the LAP/AMX nanodisks were obtained by lyophilization. The drug loading efficiency can be calculated from the following equation:

$$\text{loading efficiency} = M_t/M_0 \times 100\% \quad (1)$$

where M_t and M_0 stand for the mass of encapsulated AMX and the initial total AMX used for encapsulation, respectively.

Preparation of AMX-Loaded Electrospun Nanofibers. PLGA was dissolved in a mixed solvent of THF/DMF (v/v = 3:1) with an optimized concentration of 25% (w/v).[5] After that, AMX (0.5 wt % relative to PLGA) or LAP/AMX (with final 0.5% AMX relative to PLGA) was dispersed into PLGA solution for subsequent electrospinning to form PLGA/AMX or PLGA/LAP/AMX nanofibers, respectively (Scheme 1). PLGA/LAP nanofibers without AMX but with the same amount of LAP used to encapsulate 0.5% AMX (relative to PLGA) were also prepared as a control material. The electrospinning system was made up of a syringe pump with a 10 mL syringe, a silicone hose, a stainless steel needle with an inner diameter of 0.8 mm, a high voltage power supply, and a thin aluminum foil acting as a collector which was positioned horizontally and grounded. A clamp was used to connect the high voltage power supply with the needle. The electrospinning process was carried out under ambient condition with a fixed electrical potential of 20 kV, a collect distance of 15 cm, and a feeding rate of 0.8 mL/h by a syringe pump.[5] After electrospinning, nanofibers were taken off from the collector and vacuum-dried for at least 48 h to remove the residual organic solvent and moisture.

Characterization Techniques. The LAP and LAP/AMX nanodisks were characterized using Fourier transform infrared (FTIR) spectroscopy. The analysis was performed using a Nicolet Nexus 670 FTIR (Nicolet-Thermo) spectrometer. All spectra were recorded using a transmission mode with a wavenumber range of 650−4000 cm^{-1}. The morphology of LAP and LAP/AMX nanodisks was observed using field emission scanning electron microscopy (FESEM) (HITACHI S-4800, Japan) with an accelerating voltage of 15 kV. The LAP or LAP/AMX nanodisks were first dispersed into water. Then, the suspension of LAP or LAP/AMX nanodisks was dropped onto an aluminum foil, air-dried, and sputter-coated with a carbon film with a thickness of 10 nm before measurement. The crystalline structure of LAP, AMX, and LAP/AMX nanodisks was characterized by a Rigaku D/max-2550 PC X-ray diffraction (XRD) system (Rigaku Co., Tokyo, Japan) using Cu Kα radiation with a wavelength of 1.54 Å at 40 kV and 200 mA. The scan was performed from 5° to 60° (2θ). The plane spacing of different diffraction planes (d_{hkl}) can be calculated from the Bragg's Law:

$$d_{hkl} = \frac{\lambda}{2 \sin \theta} \quad (2)$$

where λ is the wavelength of the copper anode source (λ = 1.54 Å) and θ stands for the diffraction angle of each indexed diffraction plane. The morphology of PLGA, PLGA/LAP, PLGA/AMX, and PLGA/LAP/AMX nanofibers was observed using scanning electron microscopy (SEM) (JEOL JSM-5600LV, Japan) with an accelerating voltage of 10 kV. Before measurement, each sample was sputter-coated with a 10 nm-thick gold film. Fiber diameter was measured using Image J 1.40 G software (http://rsb.info.nih.gov/ij/down-load.html). At least 100 nanofibers from different SEM images for each sample were randomly selected and analyzed. Water contact angle test was used to evaluate the surface hydrophilicity of the PLGA/AMX and PLGA/LAP/AMX fibrous mats as reported in our previous study.[23] In brief, a pendant droplet of water with 1 μL drop size was dropped onto the surface of each sample at the randomly selected area at ambient temperature and humidity. The contact angle was measured three times for each sample using a contact angle goniometer (DSA-30, Kruss, Germany) when the droplet was stable.

In Vitro Drug Release. The in vitro release kinetics of AMX from LAP/AMX nanodisks, PLGA/AMX nanofibers, and PLGA/AMX/LAP nanofibers was studied using UV−vis spectroscopy. Briefly, LAP/AMX nanodisks (6 mg) were dispersed into 1 mL of phosphate buffered saline (PBS) solution (pH = 7.4) and placed in a dialysis bag with a molecular weight cutoff of 10 000 and then dialyzed against 2 mL of PBS solution in a sample vial. For the nanofibers, 24 mg of PLGA/AMX or PLGA/AMX/LAP nanofibers was dipped into a sample vial containing 3 mL of PBS solution. All these samples were in triplicate and were incubated in a vapor-bathing constant temperature vibrator at 37 °C for different time periods. At each time interval, 1 mL of PBS solution was taken out from each vial and an equal volume of fresh PBS solution was replenished. The optical density (OD) value was measured using a Lambda 25 UV−vis spectrophotometer at 230 nm.

In Vitro Antibacterial Activity Assay. The antibacterial activity of LAP/AMX nanodisks, PLGA/AMX nanofibers, and PLGA/LAP/AMX nanofibers was evaluated in liquid medium (2.5 g LB medium dissolved into 100 mL water) by recording the absorbance of the solution at 625 nm using a Lambda 25 UV−vis spectrophotometer, which is in direct proportion to the bacterial number.[24,25] In brief, 5 mL of the bacterial solution with an OD value of 0.1−0.2 at 625 nm was added into each 15 mL glass tube. Then, AMX powder, LAP/AMX nanodisks, PLGA/AMX nanofibers, and PLGA/LAP/AMX nanofibers were added into each tube with the AMX concentration of 10, 20, and 30 μg/mL, respectively. AMX powder was used as a positive control, while PLGA and PLGA/LAP nanofibers without AMX were used as negative controls. Tube without sample was set as another negative control. All the samples were in triplicate and incubated at 37 °C with a shaking speed of 100 rpm for 24 h. After that, the OD value at 625 nm was monitored using UV−vis spectroscopy. The bacterial inhibition percentage can be calculated by the following eqution:[26]

$$\text{bacterial inhibition } (\%) = (I_c - I_s)/I_c \times 100 \quad (3)$$

where I_c and I_s are the average ODs of the control group and the experimental group, respectively. The above method was also used to evaluate the correlation between the antibacterial activity of the PLGA/LAP/AMX nanofibers as a function of the release time. Briefly, PLGA/LAP/AMX nanofibers with the AMX mass of 100 μg were added to a glass tube containing 5 mL of the bacterial suspension with an OD value of 0.1−0.2 at 625 nm. The bacterial inhibition percentage was determined at different time points (1, 2, 6, 12, 24, 48, 72, and 96 h, respectively). For comparison, PLGA/AMX nanofibers were also tested under similar conditions.

Another antibacterial activity testing method based on solid medium was also used in this study.[27,28] Briefly, agar (1.5 g) was added into 100 mL liquid medium and autoclaved. Then, the agar medium was poured onto Petri dishes and air-dried. The PLGA, PLGA/LAP, PLGA/AMX, and PLGA/LAP/AMX nanofibrous mats were cut into small pieces with a diameter of about 1 cm and the same weight. After that, the solid agar medium plates were seeded with 100 μL of *S. aureus* suspension and covered with PLGA, PLGA/LAP, PLGA/AMX, and PLGA/LAP/AMX nanofibrous mats, respectively, for an antibacterial activity assay. In another method, the solid agar medium plates were first covered with the PLGA, PLGA/LAP, PLGA/AMX, and PLGA/LAP/AMX nanofibrous mats, respectively, and the fibrous mats were removed after a 4 h incubation. Then, 100 μL *S. aureus* suspension was seeded onto each sample-treated solid medium. All of these agar plates were incubated at 37 °C for the given time period. The bacterial inhibition zones were visually observed to test the samples' antibacterial activity.

Cytocompatibility Evaluation. For cytocompatibility evaluation, PLGA and PLGA/LAP/AMX nanofibers were prepared on coverslips with a diameter of 14 mm. Then, these mats were fixed in 24-well plates with stainless steel rings and sterilized with 75% alcohol for 2 h. After that, all wells with samples were washed 3 times with PBS solution to remove the residual alcohol. Finally, 1 mL of complete DMEM was added to individual wells to incubate at 37 °C overnight. PIEC cells were seeded at a density of 1.5×10^4 cells/well for MTT assay and 2×10^4 cells/well for SEM morphology observation, respectively. Coverslips without nanofibers and tissue culture plates (TCPs) were used as controls.

After cell seeding for 8 h or 3 days, unattached cells were washed out with PBS solution and MTT solution (40 μL) diluted with fresh medium (360 μL) was added to each well. After being incubated at 37 °C for 4 h, 400 μL of DMSO was added to dissolve the purple MTT formazan crystal. Then, 100 μL of the dissolved formazan solution of each sample was transferred into individual wells of a 96-well plate to test the OD value at 570 nm using a microplate reader (MK3, Thermo, USA). Mean and standard deviation for the triplicate wells for each sample were reported.

After being cultured for 8 h or 3 days, samples were rinsed 3 times with PBS solution and then fixed with 2.5 wt % glutaraldehyde at 4 °C for 2 h. After that, the samples were dehydrated through a series of gradient ethanol solutions of 30%, 50%, 70%, 80%, 90%, 95%, and 100% and air-dried overnight. The morphology of cells was observed by SEM (JEOL JSM-5600LV) with an accelerating voltage of 10 kV, and the samples were sputter coated with a 10 nm thick gold film before measurements.

Statistical Analysis. One-way ANOVA statistical analysis was performed to compare the cytocompatibility of cells cultured onto different materials and to compare the bacterial inhibition effect of the tested materials with different AMX concentrations in liquid medium. 0.05 was selected as the significance level, and the data were indicated with (*) for $p < 0.05$, (**) for $p < 0.01$, and (***) for $p < 0.001$, respectively.

RESULTS AND DISCUSSION

Loading of AMX within LAP Nanodisks. Different from our previous study related to the use of the lumen of HNTs for drug encapsulation,[5] the interlayer space of LAP nanodisks was used to encapsulate a model drug AMX. LAP nanodisks have a two-dimensional structure with six octahedral magnesium ions sandwiched between two layers of four tetrahedral silicon atoms,[29] and the interlayer space of LAP nanodisks has been proven to be used as a reservoir for drug encapsulation.[18−20]

The loading amount and the loading efficiency of AMX within LAP were determined using the standard concentration−absorbance (at 230 nm) calibration curve of AMX in water and was optimized by changing the concentration of LAP and AMX, respectively. As shown in Figure 1, an optimized loading efficiency of 9.76 ± 0.57% could be achieved when the AMX and LAP concentration was 2 and 3 mg/mL, respectively. It is worthwhile to note that the loading efficiency decreases with the LAP concentration, which is likely due to the prone aggregation of the LAP nanodisks at higher concentrations, leading to decreased accessibility of the drug molecules to the interlayer space of LAP. We also note that the optimized loading efficiency of 9.76 ± 0.57% may not be the highest loading efficiency; further adjusting the concentrations of LAP, AMX, and the solution pH is necessary to achieve the maximum loading efficiency.

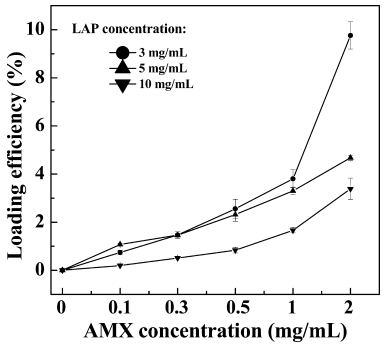

Figure 1. AMX loading efficiency as a function of AMX concentration under different LAP concentrations.

The successful encapsulation of AMX within LAP was confirmed using FTIR spectroscopy (Figure 2). In the FTIR spectrum of AMX powder (Figure 2a), the typical absorption bands at 1687, 1519, and 1235 cm^{-1} can be assigned to the amide I, amide II, and amide III bond of AMX, respectively. The weak peaks at 1770 and 1397 cm^{-1} may be attributed to the vibration of carbonyl group and carboxyl group of the AMX, respectively.[30] The peaks at 3180 and 3050 cm^{-1} are assigned to the stretching vibration of free amino group in the AMX structure. The peak of 2960 cm^{-1} can be assigned to the stretching vibration for −CH−, $-CH_2-$, or $-CH_3$ in the AMX structure. In the spectrum of LAP and LAP/AMX nanodisks (Figure 2b), the moderate peak at 1640 cm^{-1} may be caused by the moisture from the atmosphere. The strong peak located at 1012 cm^{-1} can be assigned to the −Si−O− stretching vibration of LAP naondisks,[19] and the broad peak at 3440 cm^{-1} may be due to the bending vibration of −OH in the LAP structure. By comparing the spectrum of LAP with that of LAP/AMX, a new peak emerged at 1770 cm^{-1} in the spectrum of LAP/AMX suggesting the successful encapsulation of AMX into LAP. Due to the quite low amount of AMX encapsulated within the LAP, it is difficult to observe some other distinctive peaks of AMX drug.

The morphology of LAP nanodisks before and after encapsulation of AMX was observed with FESEM (Figure S1, Supporting Information). It is clear that the disk-shaped LAP does not significantly change after the encapsulation of AMX, indicating the successful intercalation of drug molecules within the LAP interlayer space. The somewhat aggregated particles shown in the FESEM images for both samples are presumably due to the sample preparation method, which includes the air-drying process. As reported in our previous study, the air-drying of the aqueous suspension of the samples before measurement may lead to a partial aggregation or interconnection of the particles.[31]

The LAP nanodisks are able to form a stable colloidal layered structure in aqueous solution, which facilitates drug encapsulation.[32] The encapsulation of drug within the LAP interlayer space may result in a change in the interlayer distance,[33] and this can be determined by XRD technology. The XRD patterns of the LAP nanodisks before and after AMX encapsulation were compared, and the data are shown in Figure 3 and Table 1.

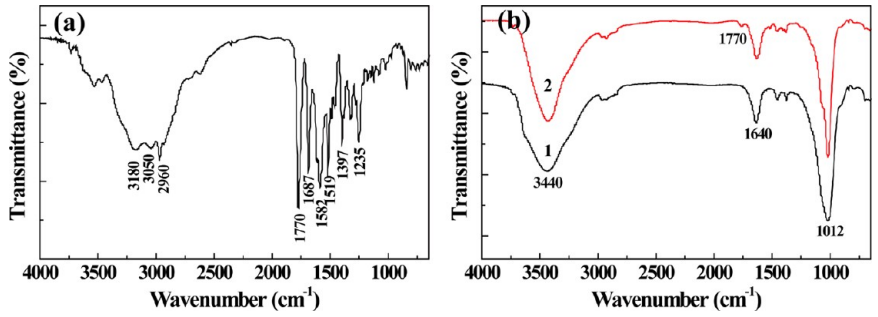

Figure 2. FTIR spectra of pure AMX (a) and LAP before (Curve 1) and after (Curve 2) AMX loading (b).

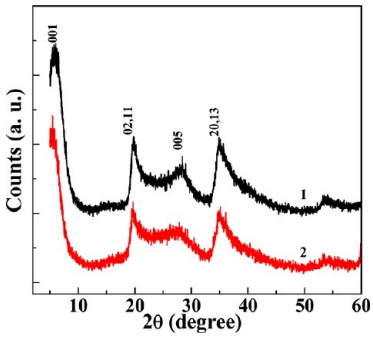

Figure 3. XRD patterns of LAP nanodisks before (Curve 1) and after (Curve 2) AMX loading.

Table 1. Diffraction Angle and Plane Spacing Data of LAP and LAP/AMX from XRD Analysis

	2θ peak position (°)		plane spacing (d, Å)	
diffraction plane (hkl)	LAP	LAP/AMX	LAP	LAP/AMX
(001)	6.06	5.50	14.76	16.26
(02,11)	19.84	19.70	4.53	4.56
(005)	28.4	27.86	3.18	3.24
(20,13)	34.88	35.12	2.6	2.59

Obviously, most of the diffraction planes at their corresponding diffraction angles do not change, suggesting that LAP is able to maintain its crystalline structure after AMX encapsulation.[34] The diffraction angle of (001) plane shifted from 6.06° to 5.50°, and the plane spacing was larger (from 14.76 to 16.26 Å) after AMX encapsulation. This is likely due to the fact that the AMX molecules are intercalated along the 001 plane. Besides, when compared with AMX powder (Figure S2, Supporting Information), no diffraction peaks of AMX can be detected in LAP/AMX nanodisks, which is presumably ascribed to the fact that the amount of the incorporated drug is too small to be detectable by the XRD technique. The XRD data suggested that the incorporation of AMX within LAP is primarily via the drug intercalation within the LAP interlayer space. It is also possible that a small portion of AMX can be adsorbed onto the LAP surface via hydrogen bonding or other weak forces.

Formation of PLGA/LAP/AMX Nanofibers. The AMX-loaded LAP was then incorporated within PLGA nanofibers (with 0.5% AMX relative to PLGA) via electrospinning to form PLGA/LAP/AMX nanofibers (Scheme 1). As controls, PLGA, PLGA/LAP (with 5% LAP relative to PLGA), and PLGA/AMX (0.5% AMX relative to PLGA) nanofibers were prepared in the same manner. The successful incorporation of LAP within PLGA nanofibers has been confirmed by thermogravimetric analysis, transmission electron microscopy, porosity measurement, mechanical testing, and contact angle measurement (see also Figure S3, Supporting Information) in our previous work.[23] Here, in this study, SEM was used to characterize the morphology of the formed electrospun nanofibers with different compositions (Figure 4). Similar to our previous studies related to the formation of PLGA/HNTs composite nanofibers,[8,35,36] we were able to form electrospun PLGA/LAP composite nanofibers with a smooth and uniform fibrous morphology even after AMX encapsulation, similar to the pure PLGA and PLGA/drug nanofibers. The diameters of PLGA/LAP (550 nm, Figure 4b), PLGA/AMX (842 nm, Figure 4c), and PLGA/LAP/AMX (591 nm, Figure 4d) nanofibers are smaller than that of pure PLGA nanofibers

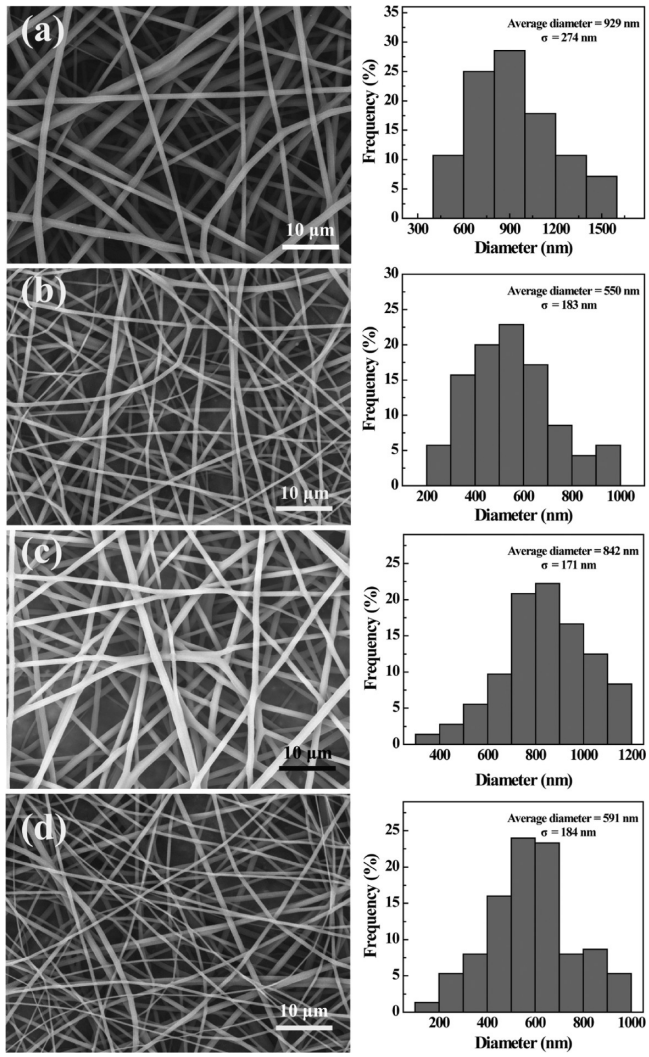

Figure 4. SEM micrographs and diameter distribution histograms of (a) PLGA, (b) PLGA/LAP (5 wt % LAP relative to PLGA), (c) PLGA/AMX (0.5 wt % AMX relative to PLGA), and (d) PLGA/AMX/LAP (5 wt % LAP relative to PLGA) nanofibers.

(929 nm, Figure 4a), presumably due to the increase of the solution conductivity, which was caused by the introduction of an anionic or a cationic species in the electrospinning solution.

Release of AMX from PLGA/LAP/AMX Composite Nanofibers. The in vitro drug release property of PLGA/LAP/AMX composite nanofibers was investigated by exposure of the fibrous mats in PBS solution (pH = 7.4) at 37 °C. The AMX release profile was compared with those from LAP/AMX nanodisks and PLGA/AMX nanofibers with similar drug content (Figure 5). It is clear that the AMX in the LAP/AMX nanodisks has a burst release profile and about 97% of the encapsulated AMX can be released from LAP within 3 h. In sharp contrast, the AMX release rate from PLGA/AMX and PLGA/LAP/AMX nanofibers was significantly reduced and showed a sustained manner. The release of AMX from PLGA/AMX nanofibers showed a moderate rate on the first day, and 31.8% of the AMX was released. Then, the release speed was slowed down, and approximately 100% drug release was achieved on the ninth day. The slower AMX release rate from PLGA/AMX nanofibers than that from LAP/AMX nanodisks is likely due to the effective hydrogen bonding and electrostatic interactions between the hydroxyl, amine, and carboxyl groups

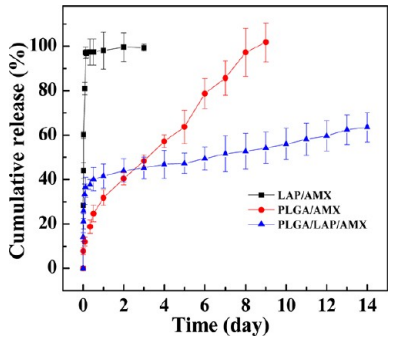

Figure 5. In vitro release of AMX from LAP/AMX nanodisks, PLGA/AMX nanofibers, and PLGA/LAP/AMX nanofibers.

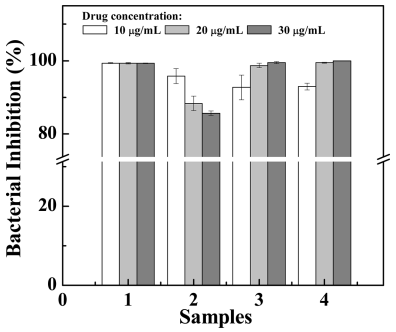

Figure 6. Growth inhibition of *S. aureus* after treatment with AMX powder (1), LAP/AMX (2), PLGA/AMX nanofibers (3), and PLGA/LAP/AMX nanofibers (4) with different AMX concentrations for 24 h at 37 °C in liquid medium.

of AMX and the carboxyl residues of PLGA polymer. The drug release profile of the PLGA/LAP/AMX composite nanofibers follows a biphasic pattern characterized by an initial fast release and a followed sustained release phase after 12 h. 40.2% of the AMX was released within the first 12 h, and a sustained release with a relatively low rate remained; 63.5% AMX was released on the 14th day. Since PLGA is biodegradable and LAP has a swelling ability in PBS solution,[23,37] it is believed that all of the encapsulated AMX can be released with time. The release rate of the PLGA/LAP/AMX nanofibers was faster than that of the PLGA/AMX nanofibers in the first 2 days and then showed a slower and sustained release rate.

The burst release of the LAP/AMX nanodisks may be due to the swelling behavior of the colloidal LAP. After contact with the PBS solution, the LAP nanodisks swell and the incorporated AMX molecules can be quickly released. The initial fast release of the PLGA/LAP/AMX nanofibers may be due to the inevitable release of AMX from LAP/AMX nanodisks when they were mixed with PLGA solution before electrospinning. After the formation of PLGA/LAP/AMX nanofibers, the partially released AMX can be attached onto the nanofiber surface or dispersed throughout the polymer matrix in a matrix-type structure, thereby causing an initial burst release. It is interesting to note that the initial burst release of PLGA/LAP/AMX nanofibers is higher than that of PLGA/AMX. This can be explained as follows: The diameter of PLGA/LAP/AMX nanofibers is apparently smaller than that of PLGA/AMX (as shown in Figure 4), which shortened the drug diffusion distance between the PLGA fiber matrix to the release medium. The followed slow release speed of the PLGA/LAP/AMX relative to the PLGA/AMX nanofibers is easily understandable due to the coexistence of two types of drug-carriers, namely, reservoir-type and matrix-type (Scheme 1). The drug should first come out from the reservoir of LAP and then from the polymer matrix, which provides an additional barrier for the drug release.[16]

In Vitro Antibacterial Activity Assay of Nanofibers. For development of novel, effective drug delivery systems, it is important to maintain the activity of the drug after encapsulation within the composite PLGA/LAP nanofibers. We next explored the in vitro antibacterial activity of the AMX-loaded nanofibers using *S. aureus* as a model bacterium both in liquid and on solid medium. Figure 6 shows the bacterial inhibition assay results of AMX powder, LAP/AMX nanodisks, PLGA/AMX nanofibers, and PLGA/LAP/AMX nanofibers in liquid medium with different AMX concentrations (10, 20, and 30 μg/mL, respectively). The AMX powder was able to inhibit the bacterial growth at each studied concentration, while the antibacterial activity of LAP/AMX nanodisks decreased with the drug concentration. This is likely due to the increased concentration of LAP in the liquid medium, which can absorb AMX molecules back to compromise the drug efficacy to some extent. The bacterial inhibition of PLGA/AMX and PLGA/LAP/AMX nanofibers increased with the drug concentration and was higher than 90% at each concentration. There was no statistically significant difference between pure AMX powder and PLGA/LAP/AMX nanofibers at the same AMX concentration in terms of the bacterial inhibition efficacy ($p > 0.05$), suggesting that the PLGA/LAP/AMX composite nanofibers have a comparable bacterial inhibition efficacy with that of the pure AMX powder. In contrast, PLGA and PLGA/LAP nanofibers without AMX encapsulation did not have any antibacterial efficacy, similar to the untreated negative control. The correlation of the antibacterial activity of PLGA/LAP/AMX nanofibers as a function of AMX release time was also investigated (Figure S4, Supporting Information). Apparently, at all the release time points (1, 2, 6, 12, 24, 48, 72, and 96 h, respectively), the released AMX from PLGA/LAP/AMX nanofibers can effectively inhibit the bacterial growth, similar to that from PLGA/AMX nanofibers.

The bacterial inhibition activity of the PLGA/LAP/AMX composite nanofibers was also tested onto solid medium. Figure 7 shows the digital photos of the antibacterial circles on agar plates at different culture times. PLGA (1), PLGA/LAP (2), PLGA/AMX (3), and PLGA/LAP/AMX (4) nanofibers were pasted onto the agar plate for bacteria inhibition (Figure 7a–c). Obviously, both the PLGA/AMX and PLGA/LAP/AMX nanofibers were able to effectively inhibit bacterial growth, and the zones of inhibition for PLGA/LAP/AMX and PLGA/AMX are basically similar in size after a 12, 24, and 48 h culture, implying that the PLGA/LAP/AMX nanofibers has a good bacterial inhibition efficacy under the studied conditions. The bacterial inhibition efficacy of the PLGA/LAP/AMX nanofibers was further confirmed by removing the nanofibrous mats from the agar plate after a 4 h release of AMX, followed by bacterial seeding (Figure 7d–f). Similar to the above method, PLGA/AMX and PLGA/LAP/AMX nanofibers were able to effectively inhibit the bacterial growth. In contrast, PLGA and PLGA/LAP nanofibers without AMX encapsulation did not inhibit the bacterial growth in both cases, implying that the bacterial inhibition effect is solely related to the encapsulated AMX drug. It should be noted that, for solid medium testing, we just tested all the nanofibrous samples because it was difficult to uniformly lay down the solid powder samples of free

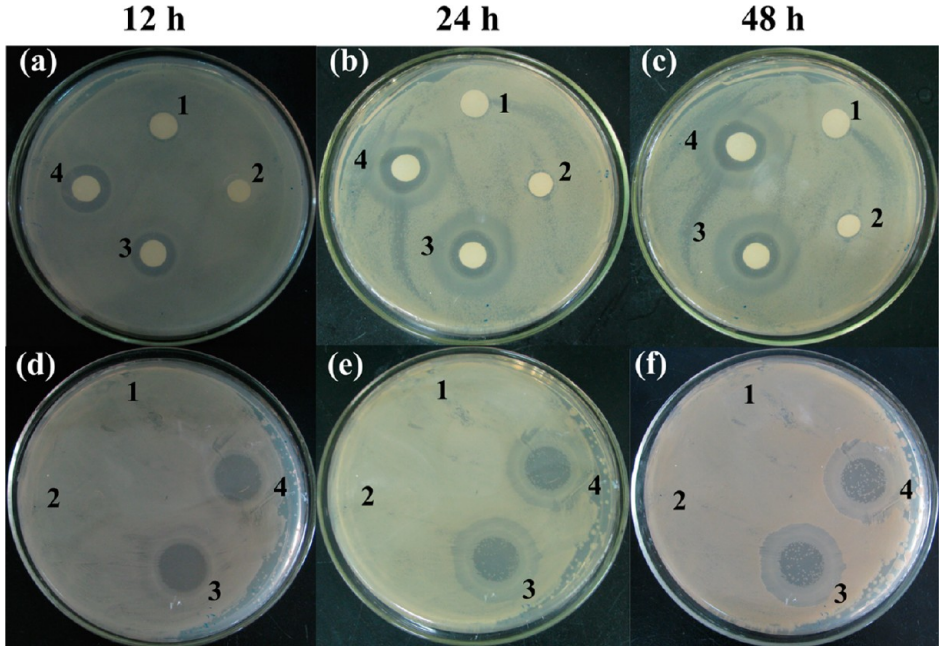

Figure 7. Inhibition of *S. aureus* cultured on agar plate incubated at 37 °C at 12, 24, and 48 h. In panels a–c, nanofibers were pasted onto the agar plate for the whole culture time period. In panels d–f, nanofibers were removed after a 4 h release of AMX onto the agar plate. 1–4 represents PLGA, PLGA/LAP, PLGA/AMX, and PLGA/LAP/AMX nanofibers, respectively.

AMX and LAP/AMX for effective comparison. Taken together with the data obtained in liquid medium, we can conclude that the developed PLGA/LAP/AMX composite nanofibers are able to inhibit the growth of a model bacterium, and the loading of AMX within the composite nanofibers does not compromise the inherent antibacterial activity of the drug. It should be noted that, although the PLGA/LAP/AMX and PLGA/AMX nanofibers showed different drug release patterns, the antimicrobial activity was almost the same. However, the major advantage of the PLGA/LAP/AMX nanofibers is that the sustained release of the drug from the fibers is very important for certain biomedical applications requiring the drug to have a long-term therapeutic efficacy. Besides, the incorporation of LAP within PLGA nanofibers can significantly enhance the mechanical property of PLGA nanofibers.[23]

Cytocompatibility of the PLGA/LAP/AMX Composite Nanofibers. To further validate the potential biomedical applications of the developed PLGA/LAP/AMX composite nanofibers, we next tested the cytocompatibility of the fibers via MTT assay in comparison with pure PLGA nanofibers with proven biocompatibility.[21,35,36] The viability of PIEC cells cultured onto both PLGA and PLGA/LAP/AMX nanofibers after 8 h and 3 days is shown in Figure 8. No statistically significant difference can be found among each sample after an 8 h culture, indicating that both PLGA and PLGA/LAP/AMX nanofibers display similar adhesion viability, in comparison with the coverslips and TCPs. On day 3, the proliferation viability of PIEC cells cultured onto both PLGA and PLGA/LAP/AMX nanofibers is significantly higher than those onto coverslips and TCPs ($p < 0.05$), and no significant difference exists between the PLGA and PLGA/LAP/AMX nanofibers ($p > 0.05$). This implies that both PLGA and PLGA/LAP/AMX nanofibers have an excellent cytocompatibility, and the incorporation of LAP/AMX nanodisks does not compromise the cytocompatibility of PLGA nanofibers. This also indicates that the released AMX at

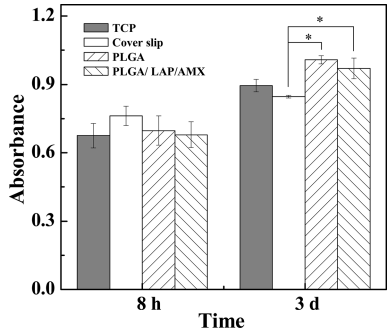

Figure 8. MTT viability assay of PIEC cells seeded on the TCPs (control), cover slips (control), PLGA nanofibers, and PLGA/LAP/AMX nanofibers (mean ± SD, $n = 3$, $^*p < 0.05$).

the time point of 8 h and 3 days does not impact the cell viability.

The comparison of the cytocompatibility of PLGA/LAP/AMX composite nanofibers with pure PLGA nanofibers was also validated via the cell morphology observation. The morphologies of PIEC cells cultured onto PLGA and PLGA/LAP/AMX nanofibers after an 8 h and 3 day culture are shown in Figure 9. Obviously, cells are able to attach onto both nanofibrous scaffolds after an 8 h culture, and after 3 days, the cells cultured onto both nanofibrous scaffolds display a phenotypic shape, indicating that the cells can penetrate and migrate within the scaffolds in a manner similar to native extracellular matrix. These cell morphology observation data corroborate the results of the MTT assay.

CONCLUSION

In summary, we developed a facile approach to encapsulating an antibiotic drug AMX within PLGA/LAP composite nanofibers for biomedical applications. The AMX-loaded LAP nanodisks with an optimized loading efficiency of 9.76 ± 0.57% were able to be incorporated within PLGA nanofibers without

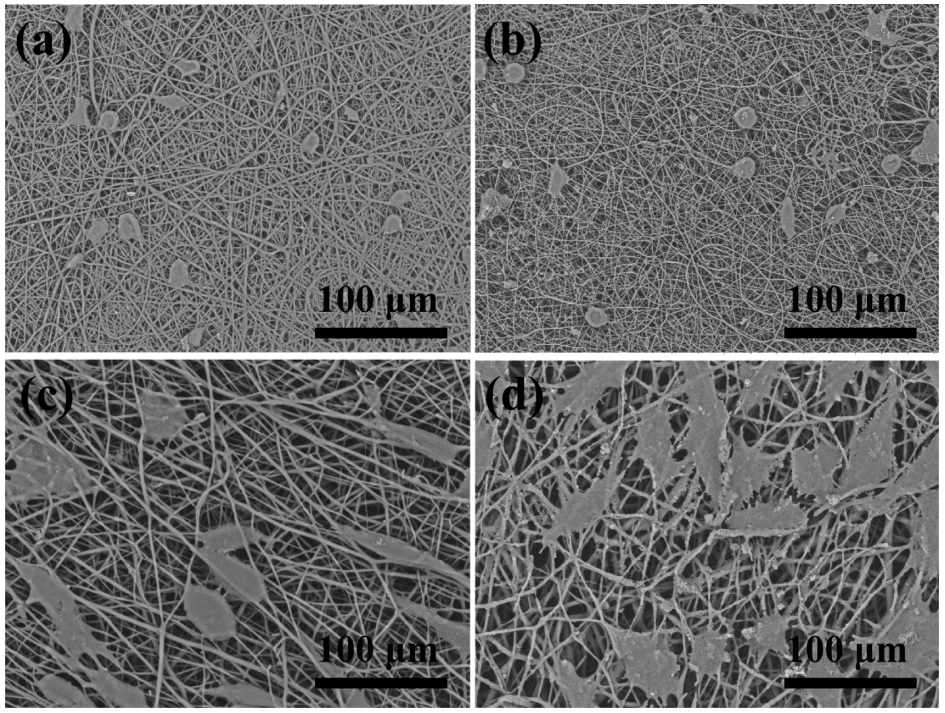

Figure 9. SEM images of PIEC cells cultured onto PLGA (a, c) and PLGA/LAP/AMX (b, d) nanofibers after an 8 h (a, b) and 3 day (c, d) culture.

significantly changing the PLGA fibrous morphology. With the coexistence of both the reservoir-type of LAP interlayer space and the matrix-type of PLGA nanofibers, the release profile of AMX was able to be significantly improved with a biphasic and sustained manner. Furthermore, PLGA/LAP/AMX nanofibers display effective antibacterial activity and noncompromised cytocompatibility in comparison with pure PLGA nanofibers. Such preparation of PLGA/LAP/AMX composite nanofibers may be able to be extended for other drug encapsulation and release for various biomedical applications in the fields of tissues engineering and pharmaceutical science.

■ ASSOCIATED CONTENT

Supporting Information

Additional materials characterization data and bacterial inhibition data. This information is available free of charge via the Internet at http://pubs.acs.org/.

■ AUTHOR INFORMATION

Corresponding Author

*E-mail: xshi@dhu.edu.cn.

Author Contributions

S.W. and F.Z. equally contributed to this work.

Notes

The authors declare no competing financial interest.

■ ACKNOWLEDGMENTS

This research is financially supported by the Program for New Century Excellent Talents in University, State Education Ministry, the High-Tech Research and Development Program of China (2012AA030309), "111 Project", B07024, and the Fundamental Research Funds for the Central Universities (for M.S. and X.S.). X.S. gratefully acknowledges the Fundação para a Ciência e a Tecnologia (FCT) and Santander bank for the Chair in Nanotechnology. S.W. thanks the Innovation Funds of Donghua University Doctorate Dissertation of Excellence (BC201107). M.Z. thanks the National Natural Science Foundation of China (50925312) for support.

■ REFERENCES

(1) Greiner, A.; Wendorff, J. H. *Angew. Chem., Int. Ed.* **2007**, *46*, 5670−5703.
(2) Li, D.; Xia, Y. *Adv. Mater.* **2004**, *16*, 1151−1170.
(3) Wang, S.; Cao, X.; Shen, M.; Guo, R.; Bányai, I.; Shi, X. *Colloids Surf., B: Biointerfaces* **2012**, *89*, 254−264.
(4) Lu, X.; Wang, C.; Wei, Y. *Small* **2009**, *5*, 2349−2370.
(5) Qi, R.; Guo, R.; Shen, M.; Cao, X.; Zhang, L.; Xu, J.; Yu, J.; Shi, X. *J. Mater. Chem.* **2010**, *20*, 10622−10629.
(6) Moreno, I.; González-González, V.; Romero-García, J. *Eur. Polym. J.* **2011**, *47*, 1264−1272.
(7) Peining, Z.; Nair, A. S.; Shengjie, P.; Shengyuan, Y.; Ramakrishna, S. *ACS Appl. Mater. Interfaces* **2012**, *4*, 581−585.
(8) Zhao, Y.; Wang, S.; Guo, Q.; Shen, M.; Shi, X. *J. Appl. Polym. Sci.* **2012**, DOI: 10.1002/APP.38054.
(9) Parajuli, D. C.; Bajgai, M. P.; Ko, J. A.; Kang, H. K.; Khil, M. S.; Kim, H. Y. *ACS Appl. Mater. Interfaces* **2009**, *1*, 750−757.
(10) Kenawy, E. R.; Bowlin, G. L.; Mansfield, K.; Layman, J.; Simpson, D. G.; Sanders, E. H.; Wnek, G. E. *J. Controlled Release* **2002**, *81*, 57−64.
(11) Shen, X.; Yu, D.; Zhu, L.; Branford-White, C.; White, K.; Chatterton, N. P. *Int. J. Pharm.* **2011**, *408*, 200−207.
(12) Yoo, H. S.; Kim, T. G.; Park, T. G. *Adv. Drug Delivery Rev.* **2009**, *61*, 1033−1042.
(13) Wang, C.; Yan, K. W.; Lin, Y. D.; Hsieh, P. C. H. *Macromolecules* **2010**, *43*, 6389−6397.
(14) Bölgen, N.; Vargel, I.; Korkusuz, P.; Menceloğlu, Y. Z.; Pişkin, E. *J. Biomed. Mater. Res., Part B* **2007**, *81*, 530−543.
(15) Xu, X.; Chen, X.; Ma, P.; Wang, X.; Jing, X. *Eur. J. Pharm. Biopharm.* **2008**, *70*, 165−170.
(16) Moghe, A. K.; Professor, B. S. G. *Polym. Rev.* **2008**, *48*, 353−377.
(17) Qi, H.; Hu, P.; Xu, J.; Wang, A. *Biomacromolecules* **2006**, *7*, 2327−2330.

(18) Jung, H.; Kim, H. M.; Choy, Y. B.; Hwang, S. J.; Choy, J. H. *Int. J. Pharm.* **2008**, *349*, 283−290.
(19) Jung, H.; Kim, H. M.; Choy, Y. B.; Hwang, S. J.; Choy, J. H. *Appl. Clay Sci.* **2008**, *40*, 99−107.
(20) Viseras, C.; Cerezo, P.; Sanchez, R.; Salcedo, I.; Aguzzi, C. *Appl. Clay Sci.* **2010**, *48*, 291−295.
(21) Liu, F.; Guo, R.; Shen, M.; Cao, X.; Mo, X.; Wang, S.; Shi, X. *Soft Mater.* **2010**, *8*, 239−253.
(22) Liu, F.; Guo, R.; Shen, M.; Wang, S. H.; Shi, X. *Macromol. Mater. Eng.* **2009**, *294*, 666−672.
(23) Wang, S.; Castro, R.; An, X.; Song, C.; Luo, Y.; Shen, M.; Tomás, H.; Zhu, M.; Shi, X. *J. Mater. Chem.* **2012**, *22*, 23357−23367.
(24) Dai, J.; Bruening, M. L. *Nano Lett.* **2002**, *2*, 497−501.
(25) Zhang, Y.; Peng, H.; Huang, W.; Zhou, Y.; Zhang, X.; Yan, D. *J. Phys. Chem. C* **2008**, *112*, 2330−2336.
(26) Kim, K.; Luu, Y. K.; Chang, C.; Fang, D.; Hsiao, B. S.; Chu, B.; Hadjiargyrou, M. *J. Controlled Release* **2004**, *98*, 47−56.
(27) Tai, Z.; Ma, H.; Liu, B.; Yan, X.; Xue, Q. *Colloids Surf., B: Biointerfaces* **2011**, *89*, 147−151.
(28) Boyle, V. J.; Fancher, M. E.; Ross, R. W., Jr. *Antimicrob. Agents Chemother.* **1973**, *3*, 418−424.
(29) Herrera, N. N.; Letoffe, J. M.; Putaux, J. L.; David, L.; Bourgeat-Lami, E. *Langmuir* **2004**, *20*, 1564−1571.
(30) Bisson-Boutelliez, C.; Fontanay, S.; Finance, C.; Kedzierewicz, F. *AAPS PharmSciTech* **2010**, *11*, 574−581.
(31) Shi, X.; Briseno, A. L.; Sanedrin, R. J.; Zhou, F. *Macromolecules* **2003**, *36*, 4093−4098.
(32) Takahashi, T.; Yamada, Y.; Kataoka, K.; Nagasaki, Y. *J. Controlled Release* **2005**, *107*, 408−416.
(33) Mercier, L.; Pinnavaia, T. J. *Microporous Mesoporous Mater.* **1998**, *20*, 101−106.
(34) Park, M.; Shim, I. K.; Jung, E. Y.; Choy, J. H. *J. Phys. Chem. Solids* **2004**, *65*, 499−501.
(35) Qi, R.; Cao, X.; Shen, M.; Guo, R.; Yu, J.; Shi, X. *J. Biomater. Sci., Polym. Ed.* **2012**, *1*, 299−313.
(36) Qi, R.; Shen, M.; Cao, X.; Guo, R.; Tian, X.; Yu, J.; Shi, X. *Analyst* **2011**, *136*, 2897−2903.
(37) Chen, M.; Gao, S.; Dong, M.; Song, J.; Yang, C.; Howard, K. A.; Kjems, J.; Besenbacher, F. *ACS Nano* **2012**, *6*, 4835−4844.